1991; Cheng et al., 1998). From the ICP-AES measurement, the Ca/P molar ratio of the HAp calcined with PAA-Ca was 1.72, and that without additives corresponded to that of stoichiometric HAp (Ca/P = 1.67). It is worth pointing out that the calcium-rich carbonate-substituted HAp had improved mechanical and biological properties compared to stoichiometric HAp (Gibson & Bonfield, 2002). We have already reported that the HAp nanocrystals, which were calcined with the anti-sintering agent, coated on a poly(ethylene terephthalate) (PET) substrate showed no cell toxicity and an improvement of cell adhesion compared to the unmodified PET substrate (Furuzono et al., 2006).

Figure 6 shows SEM and TEM photographs of the original HAp particles and the calcined HAp crystals. In the SEM photograph of the original HAp particles (Figure 6a), they had a rod-like morphology with a size ranging from 30 to 80 nm (short axis) and 300 to 500 nm (long axis). In the case of calcination without additives, some micron-sized agglomerates of polycrystals were observed, as shown in Figure 6b. On the other hand, in the case of calcination with PAA-Ca, the rod-like morphology was preserved. The higher-magnification TEM image of a particle calcined with PAA-Ca and its electron diffraction pattern (Figure 6d and e, respectively) confirmed that the particle was a single HAp crystal, and the long axis of the crystal was parallel to the *c*-axis of the HAp lattice. Other calcium phosphate phases could not be detected in the inside nor on the surface layer of the HAp crystals in Figure 6d.

The size distribution of HAp crystals and the specific surface area of the crystals are shown in Figures 7 and 8, respectively. The size distribution shown in Figure 7 was measured in an ethanol medium by DLS. In the case of calcination without additives, the mean size (1871 nm) and the specific surface area (15.5 m^2/g) of the crystals were, respectively much larger and smaller than those of the original particles before calcination (mean size, 468 nm; specific surface area, 19.6 m^2/g), which indicate the formation of agglomerates consisting of sintered polycrystals after calcination

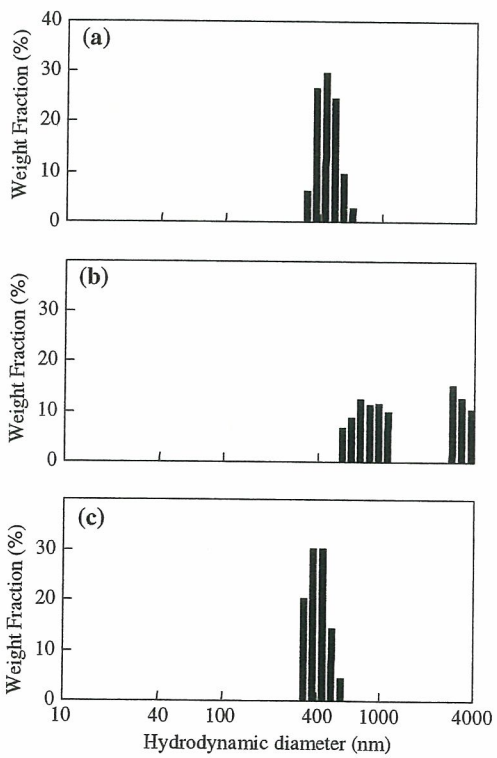

Figure 7. Size distributions of (a) original HAp particles before calcination, and HAp crystals after calcination (b) without additive and (c) with PAA-Ca. The size distributions were measured in ethanol.

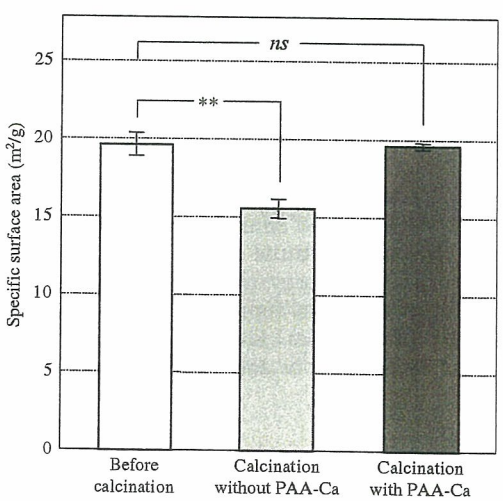

Figure 8. Specific surface areas of (a) original HAp particles, and HAp crystals after calcination (b) without additive and (c) with PAA-Ca. Error bars represent standard deviations of triplicates (**$p < 0.01$).

without additives. In the case of calcination with PAA-Ca, the size distribution (mean size, 430 nm) and the specific surface area (19.6 m^2/g) of the crystals almost corresponded to those of the original particles before calcination, respectively. In addition, the size of the HAp crystals in ethanol was close to the crystallite size in the long axis (300–500 nm) determined from the electron micrographs (Figure 6c). These results indicate that sintering between the HAp nanocrystals could be prevented by PAA-Ca surrounding the crystals prior to calcination.

Conclusion

HAp nanocrystals having a rod-like morphology were calcined at 800°C for 1 h with PAA-Ca used as the anti-sintering agent surrounding the particles, followed by removal of the agent. Although PAA-Ca was thermally decomposed during calcination, the decomposed product, CaO, remained on the particle surface. In the case of calcination without additives, some large agglomerates consisting of sintered polycrystals were observed. On the other hand, the HAp nanocrystals calcined with PAA-Ca showed high dispersibility in liquid media and a large specific surface area due to the anti-sintering effect of PAA-Ca surrounding the particles. Also, the HAp crystals calcined with PAA-Ca showed highly crystallinity, and no other calcium phosphate phases could be detected.

Acknowledgment

We thank Dr. Y. Yokogawa and Dr. K. Sato of the Advanced Manufacturing Research Institute, National Institute of Advanced Industrial Science and Technology (AIST), for helpful discussions. This work was supported by a Research Grant for Cardiovascular Diseases from the Ministry of Health, Labour and Welfare, Japan.

References

Aoki H., 1991. Science and Medical Application of Hydroxyapatite. Takayama Press System Center Co., Inc.

Barralet J.E., S.M. Best & W. Bonfield, 2000. Effect of sintering parameters on the density and microstructure of carbonate hydroxyapatite. J. Mater. Sci. Mater. Med. 11, 719–724.

Bernache-Assollant D., A. Ababoua, E. Championa & M. Heughebaertb, 2003. Sintering of calcium phosphate hydroxyapatite $Ca_{10}(PO_4)_6(OH)_2$ I. Calcination and particle growth. J. Eur. Ceram. Soc. 23, 229–241.

Bonapasta A.A., F. Buda & P. Colombet, 2001. Interaction between Ca ions and poly(acrylic acid) chains in macro-defect-free cements: A theoretical study. Chem. Mater. 13, 64–70.

Carless J.E. & A.A. Foster, 1966. Accelerated crystal growth of sulfathiazole by temperature cycling. J. Pharmaceut. Pharmacol. 18, 697–708.

Cheng Z.H., A. Yasukawa, K. Kandori & T. Ishikawa, 1998. FTIR study on incorporation of CO_2 into calcium hydroxyapatite. J. Chem. Soc. Faraday Trans. 94, 1501–1505.

Cushing B.L., V.L. Kolesnichenko & C.J. O'Connor, 2004. Recent advances in the liquid-phase syntheses of inorganic nanoparticles. Chem. Rev. 104, 3893–3946.

Emerson W.H. & E.E. Fisher, 1962. The infrared absorption spectra of carbonate in calcified tissue. Arch. Oral. Biol. 7, 671–683.

Fowler B.O., 1974. Infrared studies of apatites. I Vibrational assignments for calcium, strontium, and barium hydroxyapatites utilizing isotopic substitution. Inorg. Chem. 13, 194–206.

Furuzono T., A. Kishida & J. Tanaka, 2004. Nano-scaled hydroxyapatite/polymer composite I. Coating of sintered hydroxyapatite particles on poly(γ-methacryloxypropyl trimethoxysilane)-grafted silk fibroin fibers through chemical bonding. J. Mater. Sci. Mater. Med. 15, 19–23.

Furuzono T., K. Sonoda & J. Tanaka, 2001. A hydroxyapatite coating covalently linked onto a silicone implant material. J. Biomed. Mater. Res. 56, 9–12.

Furuzono T., P. Wang, A. Korematsu, K. Miyazaki, M. Oido-Mori, Y. Kowashi, K. Ohura, J. Tanaka & A. Kishida, 2003. Physical and biological evaluations of sintered hydroxyapatite/silicone composite with covalent bonding for a percutaneous implant material. J. Biomed. Mater. Res. B: Appl. Biomater. 65B, 217–226.

Furuzono T., M. Masuda, M. Okada, S. Yasuda, H. Kadono, R. Tanaka & K. Miyatake, 2006. Increase of cell adhesiveness on poly(ethylene terephthalate) fabric by coating of sintered hydroxyapatite nanocrystals for development of an artificial blood vessel. ASAIO J. (in press).

Gibson I.R. & W. Bonfield, 2002. Novel synthesis and characterization of an AB-type carbonate-substituted hydroxyapatite. J. Biomed. Mater. Res. 59, 697–708.

Ishikawa K., Y. Ishikawa & N. Kuwayama, 1991. Preparation of carbonate-bearing hydroxyapatites and their sintering properties. Chem. Express 6, 463–466.

Jarcho M., C.H. Bolen, M.B. Thomas, J. Bobick, J.F. Kay & R.H. Doremus, 1976. Hydroxylapatite synthesis and characterization in dense polycrystalline form. J. Mater. Sci. 11, 2027–2035.

Kawasaki T., 1991. Hydroxyapatite as a liquid chromatographic packing. J. Chromatogr. 544, 147–184.

Landi E., A. Tampieri, G. Celotti & S. Sprio, 2000. Densification behaviour and mechanisms of synthetic hydroxyapatites. J. Eur. Ceram. Soc. 20, 2377–2387.

Lim G.K., J. Wang, S.C. Ng & L.M. Gan, 1996. Processing of fine hydroxyapatite powders via an inverse microemulsion route. Mater. Lett. 28, 431–436.

Masuda Y., K. Matsubara & S. Sakka, 1990. Synthesis of hydroxyapatite from metal alkoxides through sol–gel technique. J. Ceram. Soc. Jpn. 98, 1255–1266.

Misra D.N., 1993. Adsorption of low-molecular-weight sodium polyacrylate on hydroxyapatite. J. Dent. Res. 10, 1418–1422.

Okada M. & T. Furuzono, 2006. Nano-sized ceramic particles of hydroxyapatite calcined with an anti-sintering agent. J. Nanosci. Nanotech. (in press).

Papargyris A.D., A.I. Botis & S.A. Papargyri, 2002. Synthetic routes for hydroxyapatite powder production. Key. Eng. Mater. 206–213, 83–86.

Sanchez C. & J. Livage, 1990. Sol–gel chemistry from metal alkoxide precursors. New J. Chem. 14, 513–521.

Schmidt H.K., 2000. Nanoparticles for ceramic and nanocomposite processing. Mol. Cryst. Liq. Cryst. 353, 165–179.

Schmidt H.K., E. Geiter, M. Mennig, H. Krug, C. Becker & R.-P. Winkler, 1998. The sol–gel process for nano-technologies: New nanocomposites with interesting optical and mechanical properties. J. Sol–Gel Sci. Tech. 13, 397–404.

Sindhu S. & S. Valiyaveettil, 2004. Design and synthesis of optically transparent calcium incorporated polymer complex. J. Polym. Sci. B: Polym. Phys. 42, 4459–4465.

Somiya S., K. Ioku & M. Yoshimura, 1988. Hydrothermal synthesis and characterization of fine apatite crystals. Mater. Sci. Forum 34–36, 371–378.

Sonoda K., T. Furuzono, D. Walsh, K. Sato & J. Tanaka, 2002. Influence of emulsion on crystal growth of hydroxyapatite. Solid State Ionics 151, 321–327.

Suchanek W., M. Yashima, M. Kakihana & M. Yoshimura, 1997. Hydroxyapatite/hydroxyapatite-whisker composites without sintering additives: Mechanical properties and microstructural evolution. J. Am. Ceram. Soc. 80, 2805–2813.

Taylor M.G., S.F. Parker, K. Simkiss & P.C.H. Mitchell, 2001. Bone mineral: Evidence for hydroxy groups by inelastic neutron scattering. Phys. Chem. Chem. Phys. 3, 1514–1517.

Yoshida Y., B. Van Meerbeek, Y. Nakayama, M. Yoshioka, J. Snauwaert, Y. Abe, P. Lambrechts, G. Vanherle & M. Okazaki, 2001. Adhesion to and decalcification of hydroxyapatite by carboxylic acids. J. Dent. Res. 80, 1565–1569.

Yoshimura M., H. Suda, K. Okamoto & K. Ioku, 1994. Hydrothermal synthesis of biocompatible whiskers. J. Mater. Sci. 29, 3399–3402.

Zabetakis P.M., C.M. Cotell, D.B. Chrisey & R.C. Auyeung, 1994. Pulsed laser deposition of thin film hydroxyapatite. Applications for flexible catheters. ASAIO J. 40, 869–899.

Preparation of hydroxyapatite-nanocrystals-coated stainless steel, and its cell interaction

Masahiro Okada[1], Miwa Masuda[1], Ryoichi Tanaka[2, 3], Kunio Miyatake[4], Daisuke Kuroda[5], Tsutomu Furuzono[1, *]

[1]Department of Bioengineering, Advanced Medical Engineering Center, National Cardiovascular Center Research Institute, 5-7-1 Fujishirodai, Suita, Osaka 565-8565, Japan

[2]Department of Radiology, National Cardiovascular Center, 5-7-1 Fujishirodai, Suita, Osaka 565-8565, Japan

[3]Present address: Department of Radiology, Iwate Medical University, 19-1 Uchimaru, Morioka, Iwate 020-8505, Japan

[4]National Hospital Organization Osaka Minami Medical Center, 2-1 Kido-higashimachi, Kawachinagano, Osaka 586-8521, Japan

[5]Department of Materials Science and Engineering, Suzuka National College of Technology, Shiroko-cho, Suzuka, Mie 510-0294, Japan

*Author to whom all correspondence should be addressed:

Tel: +81-6-6833-5012 (ext 2623); Fax: +81-6-6872-7485

E-mail: furuzono@ri.ncvc.go.jp

Abstract

Calcined nanocrystals of hydroxyapatite (HAp) having spherical or rod-shaped morphologies were coated through covalent linkage on a Type 316L stainless-steel substrate, which was chemically modified by the graft polymerization of γ-methacryloxypropyl triethoxysilane (MPTS) at 70–110°C. The grafting of poly(MPTS) on the substrate was confirmed by X-ray photoelectron spectroscopy (XPS) and attenuated total reflection Fourier transform infrared spectroscopy (ATR FT-IR). In order to coat the substrate with the HAp crystals through covalent linkage, the reaction between the alkoxysilyl groups in the poly(MPTS) grafted on the substrate and the OH groups on the HAp crystals was conducted at 80°C. The poly(MPTS)-grafted substrate was uniformly and strongly coated with the HAp nanocrystals, although the HAp crystals adsorbed physically on the original substrate without poly(MPTS) grafting were removed by ultrasonic treatment. Human umbilical vein endothelial cells (HUVEC) adhered in larger numbers on the HAp-coated stainless-steel substrate as compared with the original substrate, and spread to a greater extent than that on tissue culture polystyrene (TCPS) after 24 h of initial incubation. The number of HUVEC adhered on the rod-shaped HAp-coated substrate and the spherical HAp-coated substrate at the same HAp coverage ratios of 50% was not significantly different.

Key words

hydroxyapatite – nano-sized crystal – composite – covalent linkage – cell adhesion

1. Introduction

Hydroxyapatite (HAp) ceramics, a type of bioceramics, have been extensively used as implant materials for orthopedic and dental applications because they bond directly to the bone after implantation [1–5], resulting in the formation of a strong bone-implant interface. HAp ceramics have attracted attention also as a soft-tissue compatible material through the development of percutaneous devices [6]. However, owing to their mechanical weakness and brittleness, the applications of HAp ceramics have been confined to those areas for which a low mechanical stress will suffice.

We have recently developed a novel nanocomposite for a soft-tissue-compatible material [7–9]: a silk fibroin or a poly(ethylene terephthalate) fiber, whose surface was modified with nano-sized and calcined HAp crystals through covalent linkage. The novel composite nearly retained the flexibility of the polymer substrate and exhibited good tissue adhesion due to the HAp crystals on its surface [10]. The coating of the calcined HAp nanocrystals may be an effective way to improve the cell- or tissue-adhesion activity of substrates without a coating of adhesion proteins derived from animals, such as collagen and gelatin, which are intractable in terms of sterilization and storage. Recently, there have been also concerns regarding the possible role played by these proteins in infectious diseases such as bovine spongiform encephalopathy (BSE).

If our HAp nanocrystal coating technique can be applied to biomaterials other than polymer materials, its widespread application in medical fields is expected. In this regard, a metal material—Type 316L stainless steel—was selected in this study. Type 316L stainless steel is one of the most important metal biomaterials in the medical field, and has been used in artificial bones

[11], stents [12], etc. The surface modification of metal materials with HAp by the following techniques has been studied with a view to improve biocompatibility: plasma-sprayed coating [13], sputtering coating [14–15], pulsed laser deposition [16], electrochemical deposition [17], electrophoretic deposition [18, 19], treatment with simulated body fluid [20], and sol-gel coating [21]. The HAp-coating layer obtained by the above methods has an amorphous structure or low crystallinity, and the interaction at the interface between HAp and the metal surface is weak [13]. Accordingly, heat treatment around 1000°C is required to crystallize the HAp and obtain stronger interaction between HAp and the metal surface [22]. There is, however, concern regarding the effects of the high-temperature treatment on metal material and the HAp coating layer, e.g., the precipitation of carbide ($Cr_{23}C_6$) and intermetallic phases at the grain boundaries by the heat treatment of Type 316 austenitic stainless steel at 500–900°C [23]; and the metal-catalyzed degradation and shrinkage-induced cracking of the HAp layer [24].

In the present study, the above problems have been overcome by utilizing our novel coating technique for Type 316L stainless-steel substrate with calcined HAp nanocrystals through covalent linkage, which is shown in Fig. 1. The formation of covalent bonding between the HAp nanocrystals and the substrate was carried out at 80°C by a coupling reaction between the OH groups on the HAp crystal and the alkoxysilyl groups of the polymer, which was grafted on the substrate at 70–110°C. The influence of the HAp nanomorphology was evaluated by human umbilical vein endothelial cells (HUVEC) adhesion tests.

Materials and methods

Materials

The Type 316L stainless steel used in this study had a disk shape with a diameter of 12 mm and height of 3 mm, and it had the following bulk composition: C, 0.02%; Ni, 12.12%; Cr, 17.20%; Si, 0.48%; Mn, 1.39%; P, 0.33%; S, 0.24%; Fe, balance. The silane coupling agent, 3-mercaptopropyltrimethoxysilane (95% purity), was purchased from Sigma-Aldrich Co., WI, USA. γ-Methacryloxypropyl trimethoxysilane (MPTS), used as the monomer in the graft polymerization, was donated by Shin-Etsu Chemical Industries Co., Tokyo, Japan. 2,2′-azobis(isobutyronitrile) (AIBN; Nacalai Tesque Inc., Kyoto, Japan), used as the radical initiator, was purified by recrystallization. Water was purified using a Milli-Q system (Millipore Corp., Bedford, Mass.). Other materials were of reagent grade and used as purchased from Nacalai Tesque Inc.

HAp crystals with spherical or rod-shaped morphology were prepared by a wet chemical process. These HAp crystals were used after calcination at 800°C for 1 h with an anti-sintering agent surrounding the crystals to prevent the calcination-induced sintering [25–26]. The agent was removed by washing with water, and then the HAp crystals were dispersed in ethanol medium. The particle sizes measured from scanning electron microscopy (SEM) photographs (see Fig. 2) were as follows: spherical HAp nanocrystals, 73 nm (coefficient of variation (Cv), 23.1%); short axis of rod-shaped crystals, 94 nm (Cv, 26.9%); long axis of rod-shaped crystals, 401 nm (Cv, 50.2%).

Silanization of stainless-steel substrate

First, the stainless-steel substrates were cleaned ultrasonically in an acetone bath for 30 min followed by chemical treatment in a concentrated nitric acid aqueous solution for 30 min. The substrate was then thoroughly rinsed with water, and dried under N_2. The silanization of the substrate was performed at room temperature for 3 h in 10 mM ethanol solution of the silane coupling agent 3-mercaptopropyltrimethoxysilane. The silanized substrate was rinsed with ethanol and water to remove unreacted agents. It was then dried gently in N_2 and aged at 110°C for 1 h.

Graft polymerization of MPTS onto silanized stainless-steel substrate

Graft polymerization of MPTS onto the silanized stainless-steel substrate was conducted according to literature [27] as follows. The substrate was carefully immersed in a 100 mL flask equipped with an inlet for N_2, a reflux condenser, and a stirrer. Anhydrous toluene (25 mL) was added in the flask after purging N_2 for 30 min. The temperature of the mixture was raised to 70°C; 3.3 mL of MPTS monomer and 5 mL of anhydrous toluene solution containing 33 mg of AIBN were then added. The mixture was occasionally stirred during polymerization at 70°C for 2 h. Subsequently, the substrate was washed with ethanol several times to remove any homopolymers that were formed during the polymerization; finally, it was dried under reduced pressure for 1 h at 50°C.

Coating of HAp nanocrystals on stainless-steel substrate

The poly(MPTS)-grafted stainless-steel substrate was soaked in the HAp suspension (1.0 wt%) in ethanol for 1 h at room temperature so that the crystals were adsorbed on the grafted substrate. Then, the substrate was first dried under N_2, and then heated at 80°C for 2 h under vacuum (1 mmHg) in order to form covalent linkage by the reaction between the OH groups on the HAp crystals with the alkoxysilyl groups on the poly(MPTS) grafted on the substrate. The composite was washed in ethanol using an ultra sonic generator (output: 20 kHz and 35 W) for 2 min to remove the unreacted HAp crystals, which were physically adsorbed on other crystals. The composite was finally washed in a large amount of ethanol and water to remove the residual organic compounds.

Cell adhesion test

HUVEC were placed onto the HAp-coated stainless steel in 24-well multiplates at 8×10^4 cells/cm^2 in endothelial cell basal medium-2 (EGM-2; supplemented with heat-inactivated 5% fetal bovine serum (FBS) and 1 mg/mL of gentamicin/amphoterisin B) and incubated at 37°C for 24 h. The original stainless steel and a tissue culture polystyrene (TCPS) dish were used as controls.

For scanning electron microscope (SEM) observation, the samples, after incubation for 24 h, were washed twice in phosphate-buffered saline [PBS(–)]. The cells were then fixed with 10% buffered glutaraldehyde for 20 min at room temperature, followed by rinsing with PBS(–) thrice. The cells were sequentially dehydrated with aqueous ethanol (50–100%) and 100% *n*-butanol for 5 min at room temperature step by step. The samples were lyophilized and coated with gold.

The number of cells that adhered on the samples after incubation for 24 h was counted by colorimetry using Model 680 (Bio-Rad Laboratories, Inc., Tokyo, Japan) at 450 nm after staining with a water-soluble tetrazolium salt (Cell Counting Kit-8; Wako Pure Chemical Industries and Ltd., Osaka, Japan).

Measurements

The surface of the stainless-steel substrates and the cell morphologies were observed using a 5-kV SEM (JSM-6301F, JEOL, Tokyo, Japan). The surface modification of the substrate was confirmed by using attenuated total reflection Fourier transform infrared spectroscopy (ATR FT-IR; Spectrum One, Perkin-Elmer Inc., MA) at 4-cm^{-1} resolution with 16 scans, and X-ray photoelectron spectroscopy (XPS; PHI Model 1600S, Physical Electronics, Inc. MN) with a 100-W non-monochromated MgKα source at an emission angle of 45° and an investigated size of 0.8 × 2.0 mm.

Results and Discussion

A schematic diagram of the procedure for coating the stainless-steel substrate with calcined HAp nanocrystals is shown in Fig. 1. In order to covalently link the substrate and the HAp nanocrystals, the substrate was chemically modified with poly(MPTS), the alkoxysilyl groups of which can couple with the OH groups on the HAp crystal [28]. Although the physical adsorption of the MPTS homopolymer onto a substrate is the simplest method for the modification, it is not the most reliable way to obtain a poly(MPTS)-modified surface, as discussed below. Hence, the

graft polymerization was conducted in this study to covalently link the poly(MPTS) and the substrate, that is, to obtain a permanently modified surface. Prior to the graft polymerization, the substrate surface was first modified with 3-mercaptopropyltrimethoxysilane, which has mercapto groups. A mercapto group has a large transfer coefficient for radicals [29], which results in the formation of sulfur radicals on the substrate in the presence of a free-radical initiator such as AIBN. The silanization and the graft polymerization onto the stainless-steel substrate were conducted based on literature [27].

Table 1 shows the surface composition of the original, silanized, and poly(MPST)-grafted stainless-steel substrates measured by XPS. The XPS spectrum of the original substrate showed carbon and oxygen signals in addition to metal signals. The carbon signal could be attributed to the intrinsic carbon content of the steel alloy and/or the adsorption of trace amounts of hydrocarbon contaminants on the substrates. The strong O_{1s} signal in the original substrate could be attributed to hydrated oxides that covered common metals and alloys under ambient conditions. The presence of the hydrated oxides is favorable for the subsequent silanization because the coupling of a silane compound on a metal surface is considered to involve the following three steps [30, 31]: (1) hydrolysis of the silane coupling agents; (2) formation of hydrogen bonding; and (3) formation of metal-oxide bonding (M-O-Si). After the silanization of the substrate, the corresponding silicone and sulfur signals were observed in the XPS spectrum with an enhanced C_{1s} signal. The presence of metal signals suggests the formation of a thin layer of the silane coupling agent on the substrate. Following the graft polymerization of MPTS, the metal signals were not observed by XPS, suggesting the formation of a thick and uniform coating of the

poly(MPTS) on the substrate.

Fig. 3 shows the ATR FT-IR spectra of the MPTS homopolymer produced by solution polymerization under the same conditions as those in the graft polymerization, and the stainless-steel surface after the graft polymerization of MPTS. The spectrum of the MPTS homopolymer was measured after dip coating on the original stainless-steel substrate with its ethanol solution. It is noteworthy that the spectrum of the original stainless-steel substrate did not show any peaks in the same range. In the case of the MPTS homopolymer physically adsorbed on the original substrate, the Si-O-C stretching vibration of the alkoxysilyl groups was observed at 1076 cm^{-1}. On the other hand, in the case of the substrate after the graft polymerization of MPTS, the same spectrum as that in the poly(MPST) was observed. It is important to note that the poly(MPST) spectrum was observed on the grafted substrate after vigorous washing with ethanol, although the spectrum of the MPTS homopolymer physically adsorbed on the substrate disappeared after one wash with ethanol. From the above results, it was clear that the grafting of poly(MPTS) from the stainless-steel surface was well conducted.

The HAp nanocrystals, which were calcined at 800°C, were coated on the poly(MPTS)-grafted substrate through covalent linkage. Fig. 4 shows the SEM photographs of the HAp-coated substrate after ultrasonic washing. As a negative control, the original substrate, which was neither modified with the silane coupling agent nor with MPTS, was used for the modification with HAp nanocrystals. Although the HAp nanocrystals were adsorbed on the original substrate, nearly all of them were removed by the ultrasonic treatment, as shown in Fig. 4 (b). On the other hand, the crystals remained on the poly(MPTS)-grafted surface, regardless of the

morphology (spherical or rod-shaped) of the HAp crystals. The substrate was uniformly covered by the HAp nanocrystals without severe aggregations, because nearly all the nanocrystals could be dispersed in a medium by preventing the calcination-induced sintering among the crystals with the anti-sintering agent [24, 25]. Since the covalent linkage could not be observed directly on the substrate, the covalent linkage was estimated indirectly from the FT-IR analysis for the mixture of the HAp nanocrystals and MPTS homopolymer [7]. Contact atomic force microscopy also revealed that the bonding strength between the HAp nanocrystal and the poly(MPTS)-grafted surface was approximately 12 times higher than that of the original surface. The relationship between the nature of the surface and the bonding strength will be discussed in a separate publication [32].

Figs. 5 and 6 show the SEM photographs of HUVEC morphologies and the number of HUVEC on the samples after 24 h of incubation. The cover ratio of the HAp/stainless steel was controlled at around 50% by changing the concentration of HAp dispersion in the adsorption process. The cells seldom adhered on the original substrate for such a short period of incubation. On the other hand, the number of cells that adhered on the HAp-coated substrates was larger than that in the case of the original substrate (see Fig. 6). Kilpadi *et al.* showed that cell-adhesion proteins such as fibronectin and vitronectin exhibited significantly improved adsorption on HAp ceramic discs sintered at 1000°C for 3 h than on Type 316L stainless steel; this leads to the conclusion that integrins (fibronectin-binding integrin, $\alpha_5\beta_1$; vitronectin-binding integrin, $\alpha_v\beta_3$) and osteoblast precursor cells adhere significantly better on the HAp disc [33]. These observations suggest that the improved integrin-mediated cell binding may be one of the mechanisms that lead

to better cell adhesion on the HAp-coated substrates. As compared to TCPS, HUVEC on the HA-coated substrates spread to a greater extent and had pavement-like monolayer morphologies, as shown in Fig. 5. The number of cells on the HA-coated substrates, however, was lesser than that on TCPS (see Fig. 6). Although the cause of this phenomenon is unclear at present, it may be based on the more preferential adhesion of cell-adhesion proteins on the HAp-coated substrates than on TCPS, and/or the surface topography of the HAp-coated substrate, as discussed below.

Next, the influence of the HAp morphology was evaluated. As indicated above, fibronectin and vitronectin are important for cell adhesion, and these acidic proteins expected to adhere better to the *a*-plane surface of HAp; in other words, they adhere better to the rod-shaped HAp crystals elongated along their *c*-axis [25] than on spherical HAp. However, there was no difference between the number of cells and the degree of cell spreading (see Fig. 5) in the rod-shaped and the spherical HAp-coated substrates having the same surface cover ratio of HAp (50%) under the present conditions. These results suggest that the cell adhesion on a nano-sized HAp-coated surface is affected by not only the chemistry of HAp but also the surface topography such as degree of roughness and microdomain structure: cell adhesion, proliferation, and detachment strength were surface-roughness sensitive and increased with the roughness of HAp [35]; and the structure and size of the phase-separated microdomains on the block copolymer, the blocks of which had different protein adhesion properties, influenced the cell adhesion due to "capping control" of the membrane proteins on the cells [36, 37]. The topography control of HAp nanocrystal coating, such as the orientation of HAp nanocrystals and the distance between the nanocrystals on the surface, are now being attempted, and the cell-adhesion behavior on the

controlled surface will be reported in the near future.

The HAp nanocrystal coating technique is also applicable to materials with complex shapes since it is a solution process. We coated a stent (made of Type 316L stainless steel; ACTMENT Co. Ltd., Japan) with HAp nanocrystals by using the procedures described above (Fig. 7); we are now evaluating it through *in vivo* animal implantation experiments. Although Type 316L stainless-steels play a key role in metal biomaterials due to their excellent mechanical features, low cost, and ease of fabrication, they fail miserably in *in vivo* conditions due to corrosion-related problems [38] such as nickel-contact allergy [39]. Köster *et al.* have reported that patients with allergic patch-test reactions to nickel and molybdenum showed a higher frequency of in-stent restenosis than patients without hypersensitivity in a retrospective study [40], this observation suggests that allergic reactions to nickel and molybdenum ions released from stainless-steel stents may be one of the triggering mechanisms for in-stent restenosis. The HAp nanocrystal coating technique developed in this article is expected to retard the corrosion of metals because this method involves the uniform coating of the polymer layer on the metal surface.

Conclusion

A novel technique for coating Type 316L stainless-steel substrate with calcined HAp nanocrystals through covalent linkage without high-temperature treatment was developed. The coating involved three steps: (1) silanization of the substrate at 110°C; (2) graft polymerization of poly(MPTS), which could react with HAp crystals, at 70°C; (3) adsorption of HAp

nanocrystals on the substrate and reaction with alkoxyl groups in the grafted polymer on the substrate at 80°C. In a cell-adhesion test, HUVEC adhered in larger numbers on the HAp-coated substrate as compared with the original one, and spread to a greater extent than that on TCPS after 24 h of initial incubation. The number of cells that adhered and the degree of cell spreading were not different for the rod-shaped and the spherical HAp coating in the present conditions. The HAp nanocrystal coating technique is an effective way to improve the cell affinity of metal materials because it is a coating method that does not involve high-temperature treatment, and it can be applied to materials with complex shapes since it is a solution process.

5. Acknowledgment

This work was supported by a Research Grant for Cardiovascular Diseases from the Ministry of Health, Labour and Welfare, Japan.

6. References

1. Jarcho M. Calcium phosphate ceramics as hard tissue prosthetics. Clin Orthop 1981;157: 259-278.
2. Jarcho M. Retrospective analysis of hydroxyapatite development for oral implant applications. Dent Clin North Am 1992;36:19-26.
3. De Bruijn JD, Van Blitterswijk CA, Davies JE. Initial bone matrix formation at the hydroxyapatite interface in vivo. J Biomed Mater Res 1995;29: 89-99.
4. Okumura M, Ohgushi H, Dohi Y, Katuda T, Tamai S, Koerten HK, Tabata S. Osteoblastic phenotype expression on the surface of hydroxyapatite ceramics. J Biomed Mater Res 1997;37: 122-129.
5. Deligianni DD, Katsala ND, Koutsoukos PG, Missirlis YF. Effect of surface roughness of hydroxyapatite on human bone marrow cell adhesion, proliferation, differentiation and detachment strength. Biomaterials 2001;22: 87-96
6. Aoki H, Medical Applications of Hydroxyapatite, Tokyo and St. Louis, Ishiyaku EuroAmerica Inc., 1994.
7. Furuzono T, Kishida A, Tanaka J. Nano-scaled hydroxyapatite/polymer composite I. Coating of sintered hydroxyapatite particles on poly(γ-methacryloxypropyl trimethoxysilane)-grafted silk fibroin fibers through chemical bonding. J Mater Sci: Mater Med 2004;15:19-23.
8. T. Furuzono, S. Yasuda, T. Kimura, S. Kyotani, J. Tanaka, A. Kishida, Nano-scaled hydroxyapatite/polymer composite IV. Fabrication and cell adhesion properties of a three-dimensional scaffold made of composite material with a silk fibroin substrate to develop a percutaneous device, J Artif Organs 2004;7:137-144.
9. Furuzono T, Masuda M, Okada M, Yasuda S, Kadono H, Tanaka R, and Miyatake K. Increase of cell adhesiveness on poly(ethylene terephthalate) fabric by coating of sintered

hydroxyapatite nanocrystals for development of an artificial blood vessel, ASAIO J 2006;52: 315-320.

10. Furuzono T, Wang P, Korematsu A, Miyazaki K, Oido-Mori M, Kowashi Y, Ohura K, Tanaka J, Kishida A. Physical and biological evaluations of sintered hydroxyapatite/silicone composite with covalent bonding for a percutaneous implant material. J Biomed Mater Res B: Appl Biomater 2003;65B:217-226.
11. Disegi JA, Eschbach L. Stainless steel in bone surgery. Injury 2000;31:2-6.
12. Levesque J, Dube D, Fiset M, Mantovani D. Materials and properties for coronary stents. Adv Mater Process 2004;162:45-48.
13. Kangasniemi IOM, Verheyen CCPM, van der Velke EA, deGoot, K, In vivo tensile testing of fluorapatite and hydroxyapatite plasma-sprayed coatings, J Biomed Mater Res 1994;28:563-572.
14. Ong JL, Lucus LC, Lacefield WR, Rigney ED. Structure, solubility and bond strength of thin calcium phosphate coatings produces by ion beam sputter deposition. Biomaterials 1992;13:249-254.
15. Yoshinari M, Hayakawa T, Wolke JCG. Influence of rapid heating with infrared radiation on RF magnetron sputtered calcium phosphate coatings. J Biomed Mater Res 1997;37:60-67.
16. Wang CK, Lin JHC, Ju CP, Ong HC, Chang RPH. Structural characterization of pulsed laser-deposited hydroxyapatite film on titanium substrate. Biomaterials 1997;18:1331-1338.
17. Monma H. Electrochemical Deposition of Calcium-Deficient Apatite on Stainless Steel Substrate. J Ceram Soc Jpn 1993;101:737-739.
18. Sridhar TM, Subbaiyan M, Mudali UK. Preparation and characterisation of electrophoretically deposited hydroxyapatite coatings on type 316L stainless steel. Corros Sci 2003;45:237-252.

19. Mondragon-Cortez P, Vargas-Gutierrez G. Electrophoretic deposition of hydroxyapatite submicron particles at high voltages. Mater Lett 2004;58:1336-1339.

20. Kim DG, Shin MJ, Kim KH, Hanawa T. Surface treatments of titanium in aqueous solutions containing calcium and phosphate ions. Bio-Med Mater Eng 1999;9:89-96.

21. Balamurugan A, Kannan S, Rajeswari S. Electrochemical evaluation of sol-gel hydroxyapatite coatings on type 316L stainless steel-in vitro study. Can Metall Q 2004;43:293-296.

22. Ong JL, Lucas LC. Post-deposition heat treatment for ion beam sputter deposited calcium phosphate coatings. Biomaterials 1994;15:337-341.

23. Weiss B, Stickler R. Phase instabilities during high temperature exposure of 316 austenitic stainless steel. Metal Trans, 1972;3:851-866.

24. Filiaggi MJ, Pilliar RM. Interfacial characterization of a plasma-sprayed hydroxyapatite/Ti-6Al-4V implant system, in Transactions of the Tenth Annual Meeting of the Canadian Society for Biomaterials, pp.23-25 (1989)

25. Okada M, Furuzono T. Calcination of rod-like hydroxyapatite nanocrystals with an anti-sintering agent surrounding the crystals. J Nanoparticle Res, in press (Published Online at 22 July 2006)

26. Okada M, Furuzono T. Fabrication of high-dispersibility nanocrystals of calcined hydroxyapatite. J Mater Sci 2006;41: 6134-6137.

27. Zhang F, Kang ET, Neoh KG, Wang P, Tan KL. Surface modification of stainless steel by grafting of poly(ethylene glycol) for reduction in protein adsorption. Biomaterials 2001;22:1541-1548.

28. Nishizawa K, Suzuki T, Kawamoto Y, Toriyama M, Yokogawa Y, Nagata F, Tai Y, Kameyama T. Surface modification of bioceramics by silane coupling agent and their